Available online at www.sciencedirect.com

ScienceDirect

Ceramics International 39 (2013) 8773–8779

CERAMICS INTERNATIONAL

www.elsevier.com/locate/ceramint

Synthesis and characterization of spray pyrolyzed mesoporous bioactive glass

Shao-Ju Shih*, Yu-Jen Chou, Leon Valentino Posma Panjaitan

Department of Materials Science and Engineering, National Taiwan University of Science and Technology, 43, Section 4, Keelung Road, Taipei 10607, Taiwan

Received 27 March 2013; received in revised form 16 April 2013; accepted 17 April 2013
Available online 27 April 2013

Abstract

Mesoporous bioactive glasses (MBGs) have recently been applied as important bone implant materials due to their high reactive surface areas and superior bioactivities. Various processes have been developed to fabricate MBGs. Among them, the sol–gel process is one of most popular. However, sol–gel has the drawbacks of discontinuous processing and long processing time, making it unsuitable for mass production. This study demonstrates a successful synthesis of MBGs using a spray pyrolysis (SP) method to overcome these problems. The bioactivities of the SP synthesized MBGs are correlated with the main SP processing parameter of calcination temperatures and their structures. Comparisons of the surface areas and bioactivities for the MBG particles prepared from the sol–gel and the SP process are included. Finally, the MBG formation mechanism using SP is proposed.

Keywords: A. Calcination; A. Powders: chemical preparation; B. Porosity; D. Glass; E. Biomedical applications

1. Introduction

In 1971, Hench et al. first developed bioactive glasses (BGs) [1]. Since then BGs have attracted considerable attention due to their superior bioactivities and biocompatibilities. Early studies demonstrated that the surfaces of the BGs form hydroxyl apatite (HA) layers when implanted in the human body [2]. The HA layers constitute the main inorganic components of humans [3], and they are shown to chemically bond with human bones [4]. Thus, BGs have become one of the most popular materials for bone implants.

Various BGs synthesis methods have been investigated and reported. Early studies used conventional glass processes to prepare BGs [5,6]. The major advantage of the conventional glass process is its feasibility for mass production. For example, the 45S5 (SiO_2:P_2O_5:CaO:Na_2O=46.1:2.6:26.9:24.4 by molar ratio) BG® is the first commercial and most commonly available BGs. The sol–gel process for BG synthesis (firstly reported by Li et al. [2]) on the other hand, has become an popular alternate synthesis method due to the benefits of lower calcinations temperature, lower contamination and better control of chemical compositions for better bioactivities [7]. Furthermore, porous BGs have been developed to increase the specific surface area in order to achieve higher bioactivities. For example, Yan et al. [8] used tri-block surfactants of P-123 ($EO_{20}PO_{70}EO_{20}$, where EO is polyethylene oxide and PO is polypropylene oxide) and F-127 ($EO_{106}PO_{70}EO_{106}$) to prepare high surface area and well-ordered mesoporous bioactive glasses (MBGs) to improve the HA formation [8]. Although MBGs have much higher bioactivities than BGs [8,9], so far the only method to fabricate MBGs is sol–gel, which has the drawbacks of discontinuous processing, long processing time (~1–2 days) and is unsuitable for mass production [10]. In order to tackle these problems, a new MBG synthesis method is urgently needed.

Spray pyrolysis (SP) has the advantages of continuous processing and a short process time (~1 h) [11]. Recently it also has been applied to prepare borate-based BG submicron particles [12] and 45S5 BG nanoparticles [13]. However, to the best of authors' knowledge, no MBGs have been produced using SP. This report shows the first successful SP synthesized MBG particles. In addition, the relationships of calcination conditions with the particle morphologies, crystallographic structures, surface areas and bioactivities have been investigated. Since carbon contaminations caused by incomplete decomposition of precursors also affect bioactivities of the MBGs [10], the thermogravimetric analysis (TGA) method has been applied to examine decomposition

*Corresponding author. Tel.: +886 2 2730 3716; fax: +886 2 2737 6544.
E-mail addresses: shao-ju.shih@mail.ntust.edu.tw, shihsj@gmail.com (S.-J. Shih).

0272-8842/$ - see front matter
http://dx.doi.org/10.1016/j.ceramint.2013.04.064

properties of precursors and surfactants. Morphologies and particle size distributions of the particles were characterized using transmission electron microscopy (TEM) (Tecnai G2 F20, FEI, USA). Selected area electron diffraction (SAED) patterns were carried to determine the crystallographic structures. Fourier transform-infrared spectroscopy (FT-IR) spectra of the precursors and the various calcinated MBG particles were obtained to examine the potential carbon contaminations in these particles. Average pore sizes were measured from more than 50 pores in the each calcinated specimen using TEM. The surface areas of the particles were also determined using the nitrogen adsorption method (the Brunauer–Emmett–Teller (BET) method) [14] (Tristar, Micromeritics, US) and compared with the observed morphologies and carbon contaminations. For the in vitro bioactivity test, X-ray diffraction (XRD) (D2 Phaser, Bruker, US) was employed to characterize the BG particles before and after soaking in the simulated body fluid (SBF), which has ion concentrations nearly equal to those of human blood plasma [15]. The results of TEM, FT-IR, BET and XRD characterization are then correlated with the calcined conditions of the MBG particles. Based on these results, a particle formation mechanism is proposed.

2. Experimental procedures

2.1. Synthesis

The MBG particles calcinated at temperatures of 500, 600, 700 and 800 °C were prepared by SP. The precursors of the solid particles were 6.70 g tetraethyl orthosilicate (TEOS, $Si(OC_2H_5)_4$, 99.9 wt%, Showa, Japan), 1.40 g calcium nitrate tetrahydrate (CN, $Ca(NO_3)_2 \cdot 4H_2O$, 98.5 wt%, Showa, Japan) and 0.73 g triethyl phosphate (TEP, $(C_2H_5)_3PO_4$, 99 wt%, Alfa Aesar, USA). Also, the precursors were 6.7 g TEOS, 1.40 g CN, 0.73 g TEP and 7.00 g tri-block F-127 surfactant (Pluronic F-127, Sigma-Aldrich, Germany). The precursors were dissolved in 1.0 g 0.5 M HCl and 60.00 g ethanol and stirred at room temperature for 24 h. For SP, the solution (the mixture of the 10 ml precursor solution and 390 ml DI-water) was dispersed into fine droplets with the frequency of 1.65 MHz using the ultrasonic nebulizer (King Ultrasonics Co., Taiwan). Subsequently, these droplets were heated in the tube furnace (D110, Dengyng, Taiwan), with three zones of pre-heating, calcinating and cooling. In order to control pore structures, the main SP parameter of calcination temperatures (500, 600, 700 and 800 °C) was chosen to prepare various MBG powders. Also, the temperatures of the pre-heating and cooling zones were kept at 400 and 500 °C, respectively. The surface of these powders was charged by electron released from the tungsten corona wire at high voltage (16 kV). Finally the negative charged powder was neutralized and condensed in an earthed stainless steel collector.

2.2. Characterization

The decomposition behaviors of the precursor mixtures of TEOS, CN and TEP and the sufactants of F-127 were characterized by TGA (Q500, TA, USA) under an ambient airflow to remove decomposition products. The heating rate was 5 °C/min. For morphological observations, various calcined powders were first dispersed in acetone in an ultrasonic bath for 5 min, and then a drop of suspension was placed onto a lacy carbon film grid. Then, the solvent on the lacy carbon grid was evaporated at room temperature. The field emission gun TEM, operated at 200 keV, was carried out to characterize particle morphologies. The SAED patterns were recorded to check their crystallographic structures. FT-IR spectra of the precursors and the various calcined particles were obtained using a FT-IR spectrophotometer (FTS1000, Digilab, USA). For this purpose each powder was mixed with KBr (in a powder:KBr ratio of 1:20) and was pressed into a ~200 mg pellet with a 12 mm diameter. Infrared absorption spectra were obtained over the frequency range of 600–3500 cm^{-1}. Furthermore, the specific surface area data of these powders were determined by the BET method from nitrogen adsorption and desorption isotherm data obtained at −196 °C on a constant-volume adsorption apparatus. The as-prepared samples were degassed at 150 °C for 3 h before measurements. The average values and their standard deviations of the specific surface areas from a number of repeated measurements were obtained.

2.3. In-vitro bioactive test

The in-vitro bioactivity tests for the various annealed MBG particles were carried out using SBF. The ion concentrations in SBF are Na^+ 142.0, K^+ 5.0, Mg^{2+} 1.5, Ca^{2+} 2.5, Cl^- 147.8, HCO_3^- 4.2, HPO_4^{2-} 1.0, and SO_4^{2-} 0.5 mmol L^{-1} (mM). The bioactivity was tested by immersing the particles in SBF at the solid:liquid ratio of 1 g:10 ml at 37 °C for 4 h. X-ray diffractometer (D2 Phaser, Bruker, Germany), with Ni-filtered Cu Kα radiation, was used to characterized the surfaces of the various calcinated MBG particles before and after soaking in SBF.

3. Results and discussion

3.1. Precursor decomposition behavior

In order to achieve complete decomposition of precursors, SP calcination temperatures may be higher than the decomposition temperatures of precursors (measured by TGA with the heating rate of 0.083 °C/s) as the fast heating rate (100–200 °C/s) used in the SP method may not be able to reach thermodynamic equilibrium for complete decomposition. The complete decomposition is critical for avoiding carbon contamination. For this reason, further FT-IR analysis for carbon contaminations is required to confirm the suitable SP calcination temperature setting. Fig. 1 shows the thermal decomposition of the precursor mixtures of TEOS, CN and TEP as well as the surfactant, F-127. For the precursor mixtures, the major weight-loss stage in a temperature range from 50 to 400 °C can be attributed to the continuous decomposition of the precursor mixtures to form silicon dioxide, calcium oxide and phosphorus pentoxide (see Fig. 1(a)). The remaining weight percentage of the precursor mixtures (28%) was consistent with the expected value (31%). In addition, Fig. 1(b) shows the

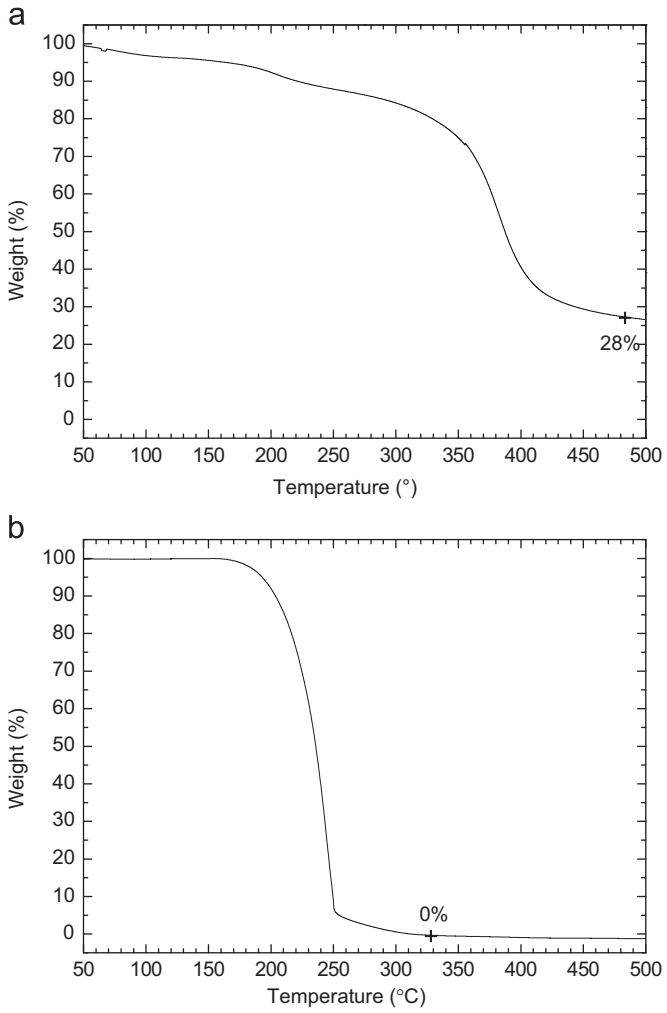

Fig. 1. TGA results of (a) the TEOS, CN and TEP precursors and (b) F-127 surfactant.

complete decomposition of the F-127 surfactants (zero weight remaining) from 150 to 330 °C. In summary, the TGA results show no indication of carbon remaining from the precursor mixtures and surfactants above 400 °C, and therefore SP temperature should be set up higher than 400 °C in this study.

3.2. Morphology and crystallographic structure

Fig. 2 shows the TEM images of the particles calcined at temperatures of 500, 600, 700 and 800 °C. The images clearly show that all the particles are spherical. The spherical morphology suggests that the precursors have high solubilities in water since the solute in the precursor droplets precipitates homogenously to generate spherical particles (i.e. volume precipitation [16]). In addition, the corresponding SAED patterns (Fig. 2 insets) present the diffused rings without any clear diffraction spots or well-defined rings, suggesting that the particles are amorphous. In these TEM images, for the specimen with a uniform composition, the image contrast is mainly associated with thickness, mass and crystal orientation, where the darker contrast represent higher thickness, mass or (close to) Bragg's conditions. In this case, the contrast is only associated with the thickness as the MBG particles are amorphous and have a uniform composition. Therefore the brighter areas are correlated with the presence of the pores. Based on our statistical analysis, the average pore sizes and their standard deviation values are 5.3 ± 1.1, 6.5 ± 0.8, 7.1 ± 1.1 and 4.9 ± 0.9 nm for particles calcined at 500, 600, 700 and 800 °C, respectively. The combined TEM and SAED results conclude that these particles are glassy (amorphous) and spherical shaped and mesoporous. Also, BET has been carried out to confirm the porosity.

Both the particle size [13] and particle porosity [17] govern the surface areas and therefore both have effect on the bioactivities of the bioglasses. For simplification, this study attempted to control the particle sizes, in order to investigate how mesoporous structures (e.g. pore size) affect the bioactivities. To control the particle size, the same solution concentration and ultrasonic frequency were applied to the particles calcined at various temperatures, since it has been shown that solution concentration and ultrasonic frequencies determine the particle sizes [18]. Fig. 3 shows the size histograms for the MBG particles calcined at 500, 600, 700 and 800 °C with their average diameters of 624 ± 335, 701 ± 406, 618 ± 317 and 573 ± 322 nm, respectively. This result reveals that these particles have a similar size and distribution, and therefore surface areas of this study are mainly contributed by the mesopores.

In order to confirm whether carbon contamination (i.e. incomplete decomposition of precursors) existed in the MBG particles, FT-IR has been employed. The FT-IR spectra in the 3300–600 cm^{-1} range of the precursors and the calcined particles are shown in Fig. 4. The spectrum of the precursors show several features attributed to silicates (~800, ~850, and ~1100 cm^{-1} for Si–O–Si) [19,20], phosphates (970 cm^{-1} for P–O and 1030 cm^{-1} for PO_4^{3-} [19]), carbon oxide (~1430 cm^{-1} for CO_3^{2-} and ~2350 cm^{-1} for CO_2 [21]), carbonates (C–C for 2900 cm^{-1} and CH_2 for 3000 cm^{-1} [22]) and residual water (OH for ~1630 cm^{-1} [20]). The MBG particles calcined at 500 and 600 °C contain most peaks in the spectrum of precursors including silicates, phosphates, carbon oxide and residual water except carbonates. The presence of the carbonate indicates carbon contamination due to incomplete decomposition of precursors (Fig. 4). This result does not conflict with TGA result because the heating rate of SP is much faster than that of TGA. When the particles are calcined to 700 and 800 °C, there is no indication of carbonates in FT-IR spectra (Fig. 4). In summary, residual carbonates decompose completely when SP calcination temperature is above 700 °C.

3.3. Specific surface area

It is established that the surface area dominates bioactivities of bioglasses [21]. The BET data reveal that the specific surface areas of the MBG particles calcinated at 500, 600, 700 and 800 °C are 121.8 ± 0.2, 136.4 ± 0.6, 261.3 ± 0.9 and 211.8 ± 1.3 m^2/g, respectively, as shown in Fig. 5. The surface area increases with increasing calcination temperatures, and it reaches the maximun value at 700 °C. The surface area of the MBG particles shows a decrease of ~18.9% (~49 m^2/g) when calcined from 700 to 800 °C. Likewise, the pores' sizes

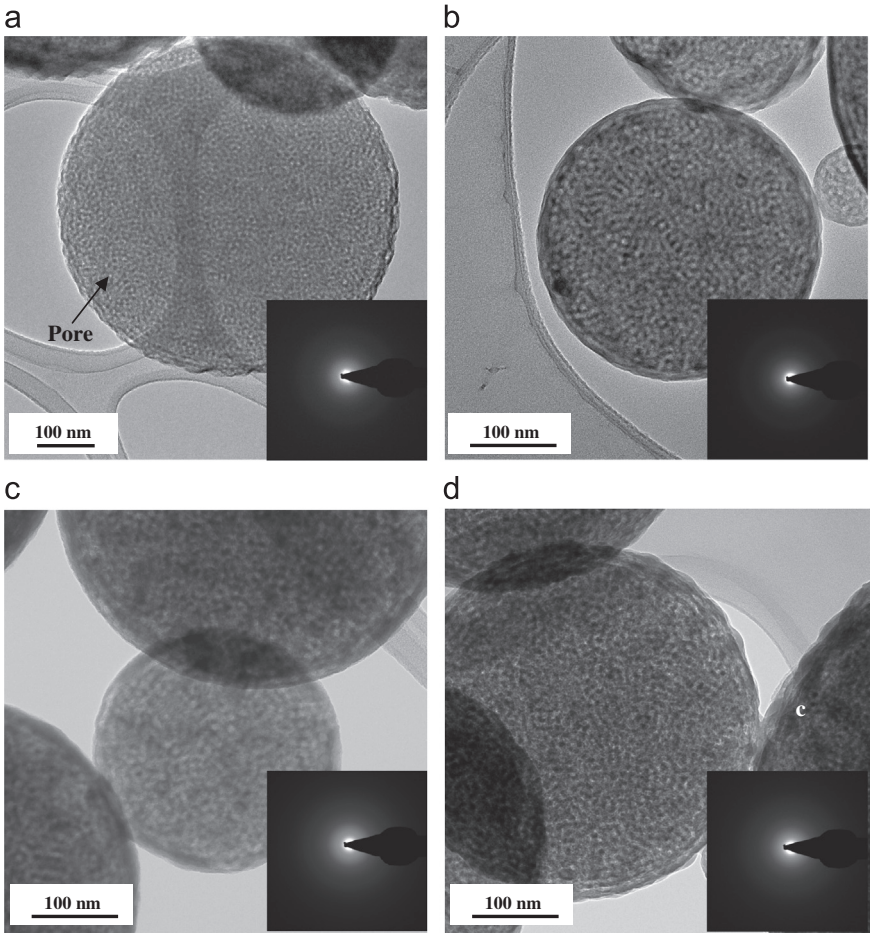

Fig. 2. Microstructures of the MBG particles calcinated at the temperatures of (a) 500, (b) 600, (c) 700 and (d) 800 °C. SAED patterns of the various calcinated MBG particles are in (a)–(d) are shown as insets in the corresponding images.

determined from the TEM images shown in Fig. 2 (discussed previously) follow a similar trend: it slightly increases with increasing calcination temperature and reaches a maximun value at 700 °C, and the pore size then decreases for ~30.9% from 700 to 800 °C. The decrease of surface area from 700 °C to 800 °C may be due to pore shrinkage (7.1 nm for 700 °C and 4.9 nm for 800 °C), as supported by the particle diameter shrinkage (618 nm for 700 °C and 573 nm for 800 °C). Although the particles calcined at 600 and 700 °C have a similar pore size (6.5 ± 0.8 nm for 600 °C and 7.1 ± 1.1 nm for 700 °C), the surface area of the particles calcined at 700 °C (261.3 ± 0.9 m^2/g) is two times larger than that at 600 °C (136.4 ± 0.6 m^2/g). This result may be due to the carbon contamination covering some pores in the particles calcined at 600 °C, resulting in the surface area reduction.

3.4. In-vitro bioactive test for bioactive glass

Fig. 6 shows the XRD patterns of the calcinated MBG particles before and after immersing in SBF for 4 h. The XRD patterns of the MBG particles confirm the absence of any crystalline phases (amorphous) before soaking: no diffraction maximum is observed and only a broad band between 20° and 37° is apparent, as shown in Fig. 6(a). After immersing in SBF for 4 h, as shown in Fig. 6(b), four diffraction peaks appear at 31.9°, 45.6°, 56.6° and 75.4°, corresponding to the (211), (222), (322) and (432) planes of HA (JCPDF number of 84-1998). Bioactivities are directly related to the crystal growth rates of HA in SBF. In order to minimize the errors, the (211) peaks have been chosen for HA crystal size estimation using Scherrer's formula [23]. The HA crystal sizes for the particles calcined at 500, 600, 700 and 800 °C are 14.9, 17.2, 35.2 and 21.5 nm, respectively, suggesting that the bioactivities of the MBG particles follow the order of 700 °C > 800 °C > 600 °C > 500 °C. This trend agrees well with the order of specific surface area (700 °C > 800 °C > 600 °C > 500 °C), suggesting that the higher specific surface area does enhance bioactivities for the MBGs. Based on the experimental results of TEM, FT-IR, BET and the in-vitro bioactive tests (XRD), the SP particles calcinated at 700 °C produce the carbon contamination free MBG particles with a higher specific surface area and a better bioactivity.

3.5. Morphology formation

Fig. 7 shows a schematic diagram of the MBG formation mechanism. The precursor mixtures of TEOS, CN and TEP are orientated randomly with the F-127 surfactant in droplets.

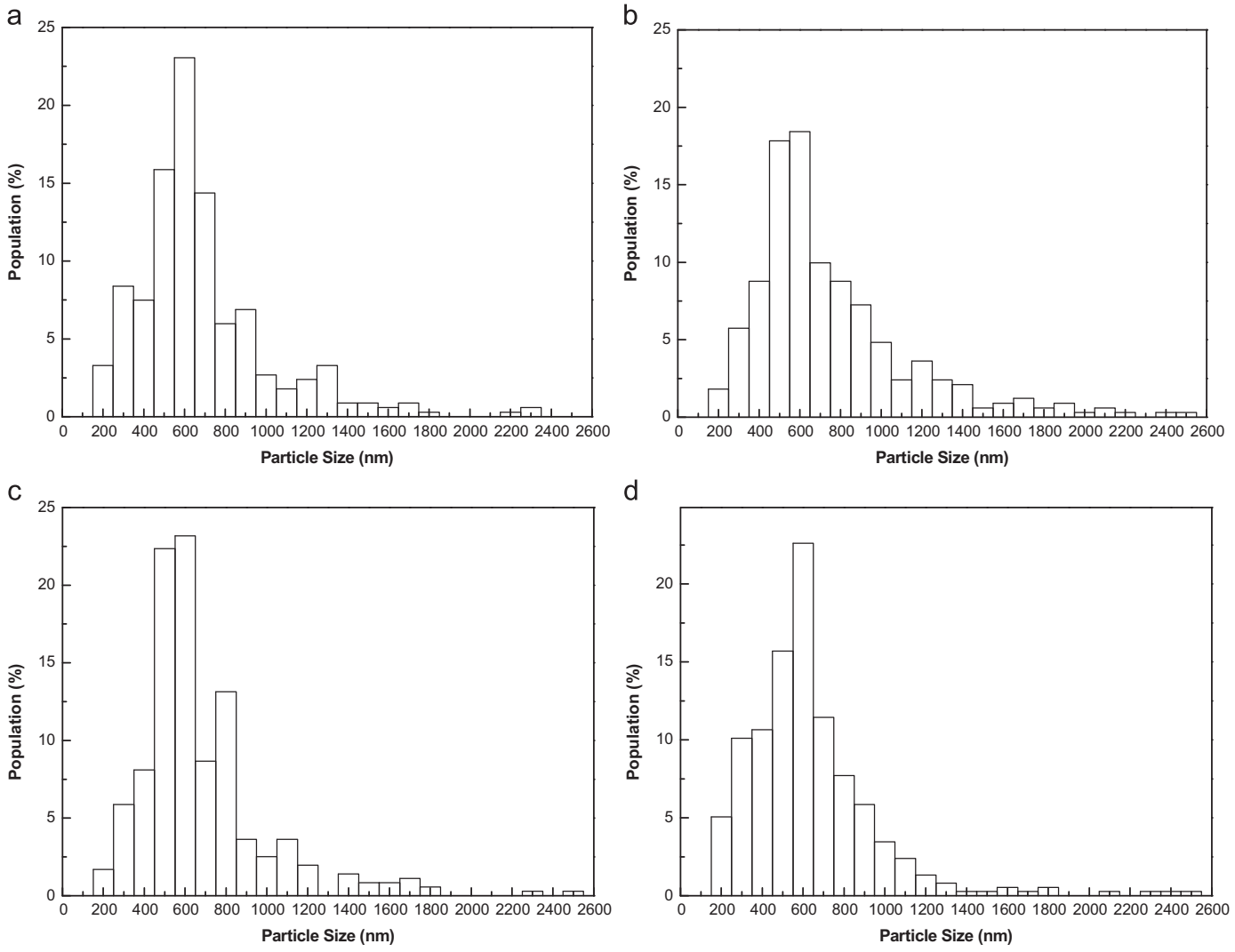

Fig. 3. Particle size histograms of the MBG particles calcinated at the temperatures of (a) 500, (b) 600, (c) 700 and (d) 800 °C.

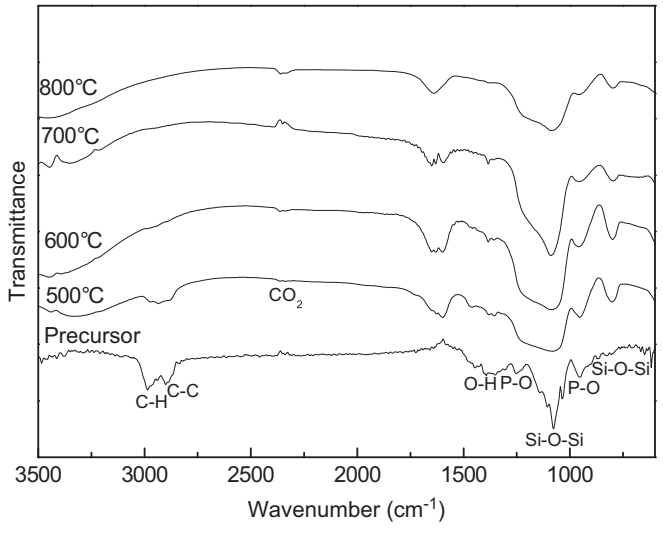

Fig. 4. FTIR spectra of the MBG particles calcinated at the temperatures of 500, 600, 700 and 800 °C.

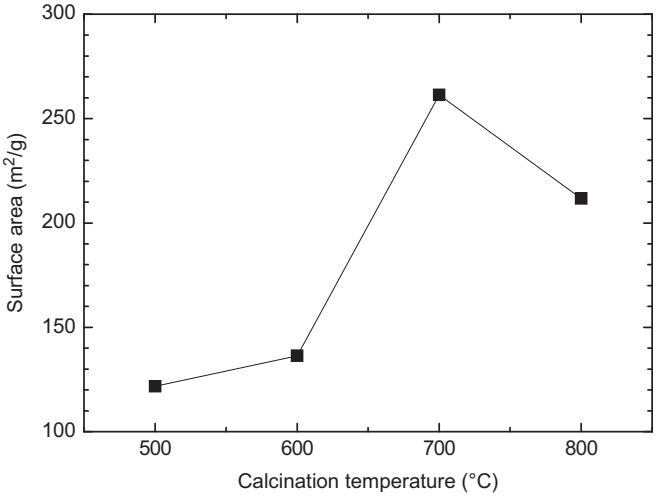

Fig. 5. Surface areas of the MBG particles with calcination temperatures of 500, 600, 700 and 800 °C.

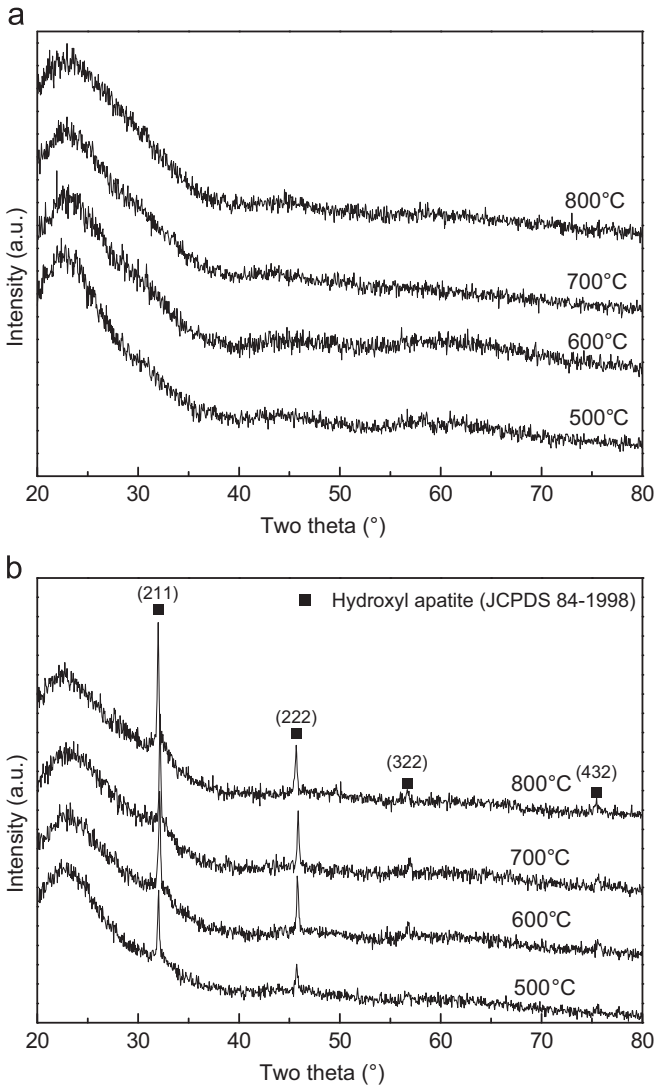

Fig. 6. The XRD patterns of the MBG particles (a) before and (b) after soaking in SBF solution for 4 h. The indexed peaks belong to the HA phase (JCPDF number of 84-1998).

These surfactants in the droplets form micelles when they reach a critical concentration in the atomization stage [24]. For these micelles, the hydrophilic PO groups gather outside, whereas the hydrophobic EO groups gather inside. The micelles aggregate themselves to form a supramicellar structure [24], and the TEOS, CN and TEP precursors are subsequently surrounded by hydrophilic PO groups (outside of the micelles), as shown in Fig. 7. After the stages of evaporation, decomposition and calcination, these micelles form a porous framework for the MBG particles.

We have conducted comparisons of the surface area and bioactivities between the SP derived particles and the sol–gel derived particles with the same chemical composition [10]. Firstly, for the same surfactant concentration, the SP particles have a lower surface area (121.8–261.3 m^2/g in this study) compared to that of the sol–gel particles (320.0–469.2 m^2/g). The pores are irregularly arranged in the SP particles (Fig. 2) due to the rapid calcination time (~10 s), whereas the pores in the sol–gel particles are ordered (hexagonal arrangements) due to the longer calcination time (~2–6 h) [9,10]. Secondly, for the same SBF immersing time (4 h in SBF), the HA crystal size is 35.9 nm (with surface area of 261.3 m^2/g) for the SP particles, which is much larger than that (~4.0 nm (obtained from the XRD pattern in Ref. [10] using Scherrer's formula)) for the sol–gel particles (with surface area of 328.0 m^2/g). This comparison suggests that the SP particles have higher HA formation rate than that of the sol–gel particles. The reason why the SP articles have higher bioactivity than the sol–gel particles even though the SP particles have lower surface area is described as follow. SP process offers a faster cooling rate than that of sol–gel, and therefore the process favors the existence of the metastable siloxane [25]. The presence of the siloxane provides more nucleation sites for the formation of HA layers and therefore gives higher bioactivities [26]. Therefore the SP particles have superior bioactive properties than that of the sol–gel particles although the SP particles have less surface area than that of the sol–gel particles.

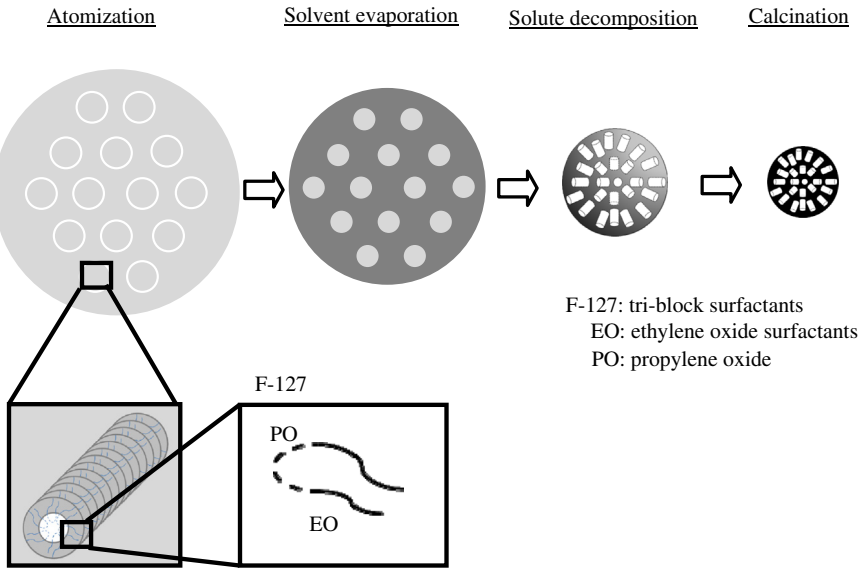

Fig. 7. The schematic diagram of the MBG particles prepared using SP.

4. Conclusions

This study reports the first synthesis of the MBG particles using the SP process. The study also correlates the morphologies, crystallographic structures, chemical compositions, specific surface areas with the bioactivities of MBG particles at various calcination conditions. With increasing calcination temperatures, the pore size and surface area reach the maximum values at 700 °C and then decrease at 800 °C. The in-vitro bioactive tests confirm that the particles calcined at 700 °C have the highest surface area, highest HA formation rate and therefore better bioactivities. Finally, this study proposes a formation mechanism for the MBGs synthesized using the SP method, contributing to an improved synthesis method to this important materials for bone implants.

Acknowledgments

The authors acknowledge the financial support from National Taiwan University of Science and Technology (Grant no. 100H451201) and the National Science Council of Taiwan (Grant no. NSC 101-2628-E-011-008-MY2).

References

[1] L.L. Hench, R.J. Splinter, W.C. Allen, T.K. Greenlee, Bonding mechanisms at the interface of ceramic prosthetic materials, Journal of Biomedical Materials Research 5 (1971) 117–141.
[2] R. Li, A.E. Clark, L.L. Hench, An investigation of bioactive glass powders by sol–gel processing, Journal of Biomaterials 2 (1991) 231–239.
[3] W. Xia, J. Chang, Preparation, in vitro bioactivity and drug release property of well-ordered mesoporous 58S bioactive glass, Journal of Non-Crystalline Solids 354 (2008) 1338–1341.
[4] M. Vallet-Regi, Ceramics for medical applications, Journal of the Chemical Society: Dalton Transactions (2001) 97–108.
[5] W. Vogel, W. Höland, Nucleation and crystallization kinetics of an $MgO–Al_2O_3–SiO_2$ base glass when using different doping agents, Zeitschrift fuer Chemie 22 (1982) 429–438.
[6] W. Vogel, W. Höland, K. Naumann, J. Gummel, Development of machineable bioactive glass ceramics for medical uses, Journal of Non-Crystalline Solids 80 (1986) 34–51.
[7] L.L. Hench, Sol–gel materials for bioceramic applications, Current Opinion in Solid State and Materials Science 2 (1997) 604–610.
[8] X.X. Yan, C.Z. Yu, X.F. Zhou, J.W. Tang, D.Y. Zhao, Highly ordered mesoporous bioactive glasses with superior in vitro bone-forming bioactivities, Angewandte Chemie International Edition 43 (2004) 5980–5984.
[9] W. Xia, J. Chang, Well-ordered mesoporous bioactive glasses (MBGs): a promising bioactive drug delivery system, Journal of Controlled Release 110 (2006) 522–530.
[10] C.J. Shih, H.T. Chen, L.F. Huang, P.S. Lu, H.F. Chang, I.L. Chang, Synthesis and in vitro bioactivity of mesoporous bioactive glass scaffolds, Materials Science and Engineering C: Materials for Biological Applications 30 (2010) 657–663.
[11] S.J. Shih, L.Y.S. Chang, C.Y. Chen, K.B. Borisenko, D.J.H. Cockayne, Nanoscale yttrium distribution in yttrium-doped ceria powder, Journal of Nanoparticle Research 11 (2009) 2145–2152.
[12] J.S. Cho, Y.C. Kang, Synthesis of spherical shape borate-based bioactive glass powders prepared by ultrasonic spray pyrolysis, Ceramics International 35 (2009) 2103–2109.
[13] M. Mačković, A. Hoppe, R. Detsch, D. Mohn, W.J. Stark, E. Spiecker, A.R. Boccaccini, Bioactive glass (type 45S5) nanoparticles: in vitro reactivity on nanoscale and biocompatibility, Journal of Nanoparticle Research 14 (2012) 966.
[14] S. Brunauer, P.H. Emmett, E. Teller, Adsorption of gases in multimolecular layers, Journal of the American Chemical Society 60 (1938) 309–319.
[15] T. KuKubo, S. Ito, Z.T. Huang, T. Hayashi, S. Sakka, T. Kitsugi, T. Yamamuro, Ca, P-rich layer formed on high strength bioactive glass-ceramic A-W, Journal of Biomedical Materials Research 24 (1990) 331–343.
[16] G.L. Messing, S.C. Zhang, G.V. Jayanthi, Ceramic powder synthesis by spray-pyrolysis, Journal of the American Ceramic Society 76 (1993) 2707–2726.
[17] B. Lei, X.F. Chen, Y.G. Wang, N.R. Zhao, C. Du, L.M. Fang, Synthesis and bioactive properties of macroporous nanoscale $SiO_2–CaO–P_2O_5$ bioactive glass, Journal of Non-Crystalline Solids 355 (2009) 2678–2681.
[18] Y.L. Song, S.C. Tsai, C.Y. Chen, T.K. Tseng, C.S. Tsai, J.W. Chen, Y.D. Yao, Ultrasonic spray pyrolysis for synthesis of spherical zirconia particles, Journal of the American Ceramic Society 87 (2004) 1864–1871.
[19] S. Agathopoulos, D.U. Tulyaganov, J.M.G. Ventura, S. Kannan, M.A. Karakassides, J.M.F. Ferreira, Formation of hydroxyapatite onto glasses of the $CaO–MgO–SiO_2$ system with B_2O_3, Na_2O, CaF_2 and P_2O_5 additives, Biomaterials 27 (2006) 1832–1840.
[20] B.A. Allo, A.S. Rizkalla, K. Mequanint, Hydroxyapatite formation on sol–gel derived poly(epsilon-caprolactone)/bioactive glass hybrid biomaterials, ACS Applied Materials and Interfaces 4 (2012) 3148–3156.
[21] Z.M. Li, X.F. Chen, C. Lin, N.R. Zhao, The in vitro bioactive of sol–gel bioactive glass powders with three-dimensional lamellar structure, Advanced Powder Technology 23 (2012) 13–15.
[22] P. Innocenzi, P. Falcaro, D. Grosso, F. Babonneau, Order–disorder transitions and evolution of silica structure in self-assembled mesostructured silica films studied through FTIR spectroscopy, Journal of Physical Chemistry B 107 (2003) 4711–4717.
[23] B.D. Cullity, S.R. Stock, Elements of X-ray Diffraction, Prentice-Hall, Inc., New Jersey, 167–171.
[24] M. Vallet-Regi, F. Balas, M. Colilla, M. Manzano, Bone-regenerative bioceramic implants with drug and protein controlled delivery capability, Progress in Solid State Chemistry 36 (2008) 163–191.
[25] W.P. Cao, L.L. Hench, Bioactive materials, Ceramics International 22 (6) (1996) 493–507.
[26] L.L. Hench, J.K. West, Bioceramics, Butterworth-Heinemann Ltd., Oxford, 35–40.